Effect of Multi-Walled Carbon Nanotubes Incorporation on the Structure, Optical and Electrochemical Properties of Diamond-Like Carbon Thin Films

H. Zanin,[a,b,z] P. W. May,[b] A. O. Lobo,[c] E. Saito,[a] J. P. B. Machado,[a] G. Martins,[a] V. J. Trava-Airoldi,[a] and E. J. Corat[a]

[a]*National Institute for Space Research, 12227-010 São Jose dos Campos, São Paulo, Brazil*
[b]*School of Chemistry, University of Bristol, Bristol BS8 1TS, United Kingdom*
[c]*Laboratory of Biomedical Nanotechnology, Institute of Research and Development at the UNIVAP, 12244-000 São José dos Campos, São Paulo, Brazil*

We report the effect of incorporation of multi-walled carbon nanotubes (MWCNT) on the mechanical, structural, optical and electrochemical properties of diamond-like carbon (DLC) thin films. The DLC/MWCNT hybrid composite was deposited onto stainless steel and quartz substrates by plasma enhanced chemical vapor deposition at low temperature (∼100°C). Raman spectra of DLC/MWCNT film have characteristics from both DLC and MWCNT. The optical bandgap energy decreases with the incorporation of nanotubes. Scanning electron microscopy images confirm the presence of the MWCNT within the DLC film, forming a large interconnected conducting mesh. Tribological tests confirm there was slight adherence loss with incorporating MWCNT into the DLC films, while improving their electrical conductivity. Electrochemical assays show the incorporation of MWCNT converts DLC from an insulating material into a reversible electrode with fast charge transfer. This novel hybrid composite is shown to be mechanically robust, chemically inert and exhibits fast charge-transfer kinetics, which is very promising for several new applications.
© 2014 The Electrochemical Society. [DOI: 10.1149/2.011405jes] All rights reserved.

Among carbon-based materials, diamond-like carbon (DLC) is a metastable form of amorphous carbon, containing tetrahedral (sp^3) and trigonal (sp^2) carbon hybridisations.[1] DLC has a wide range of properties, such as high electrical resistivity, high hardness, chemical inertness, and low friction coefficient,[1–3] which can often be controlled by changing the deposition conditions. The major use of DLC is for protective coatings,[1] for example: as a solid lubricant, and as a hard-wearing layer on cutting tools. Usually DLC films are electrically insulating, however many more applications would be possible if the DLC films were electrically conductive. There are several reports of attempts improve the electrical conductivity of DLC by adding n- and p-type dopants.[2,4–9,10–13] Common dopants investigated include light elements (B, N, I, S, or F), metals, and combinations of these, and results show that these dopants changed the electrical conductivity as required, but also produced unwanted changes in the hardness, tribological properties, internal stress, adherence, and biocompatibility of the films.[10,11] For example, incorporation of metals into DLC usually reduces the film stress or increases the hardness and toughness; however, they can make the film opaque.[2] Using micro-hardness tests, Allon-Alaluf et al. reported decreased micro-hardness after DLC nitrogen and iodine doping.[12] Wei and co-workers researched mechanical, electrical, and optical properties of DLC doped with copper, titanium, and silicon elements. They showed that the incorporation of those metals could change the DLC conduction type, improve the free carrier and the localized state contributions, and make the films a black-body radiator.[13,14]

Rather than dope the DLC with another element, a better option might be to incorporate conducting forms of carbon, such as carbon nanotubes (CNTs), into the DLC. Only a few papers[15–17] report attempts to combine multiwall (MW) CNTs and DLC to create an all-carbon hybrid material. Hu et al.[15] reported that the incorporation of MWCNTs into DLC decreased the internal stress and increased the hardness and elasticity of the carbon films. Kinoshita et al.[17] described the deposition of DLC onto silicon with high densities (from $1–7 \times 10^9$ cm^{-2}) of vertically aligned CNTs. They noted that the film toughness increased; and the dynamic hardness and elastic modulus decreased linearly with increasing MWCNT density. Wei et al. developed a theoretical model for DLC/CNT composites and suggested that the orientation of the CNTs within the film is more critical for hardness improvement than the number of CNTs incorporated.[18]

All of these reports concern the effect upon the DLC mechanical properties with CNT incorporation. To the best of our knowledge, this paper shows for the first time the effects of MWCNT incorporation on the optical, structural, and electrochemical properties of DLC thin films. Electrochemical techniques have been reported to characterize a number of DLC thin films. Liu and co-workers fabricated nitrogenated DLC electrodes, and reported their superior electrochemical properties, such as wide potential window and low background current.[19] Also they showed that undoped DLC films improve corrosion resistance.[20] Maalouf et al. described the performance of nickel-doped DLC electrodes for hydrogen peroxide detection.[21] Kim and co-workers prepared microelectrodes of boron-doped DLC and its electrochemical performance for medical diagnosis was evaluated.[22] Schnupp et al. showed that thin DLC electrodes may have a nearly ideal reversibility for a redox couple, which is promising for electrochemical and bio-electronic applications.[23]

In this paper we show a simple route to prepare DLC/MWCNT hybrid composites which are mechanical robust, chemically inert and which exhibit fast charge-transfer kinetics on their surface.

Experimental

The MWCNTs were prepared using a mixture of camphor (85% wt) and ferrocene in a thermal chemical vapor deposition (CVD) furnace, as reported elsewhere.[24] The mixture was vaporized at 220°C in an antechamber, and then the vapor was carried by an argon gas flow at atmospheric pressure to the CVD furnace chamber set at 850°C. The CVD growth took only a few minutes and produced black powder, which consisted of CNT with 20–50 nm diameter and up to 40 μm length.[25]

The DLC films were deposited using a pulsed-DC discharge under controlled conditions to gain maximum hardness, minimum stress, and a maximum deposition rate.[26] DLC films (1 μm thick) were deposited onto AISI F138 stainless steel plates (20 mm × 10 mm). To guarantee adherence, the substrates were first polished and then cleaned in an ultrasonic bath in isopropyl alcohol for 5 min. After drying, the substrates were introduced into the plasma enhanced chemical vapor deposition (PECVD) reactor, and pumped down to a base pressure of ∼10^{-4} Pa to guarantee minimal oxygen in the reactor chamber. A schematic diagram of the experimental setup is presented in Figure 1.

For all steps described below, DC pulses of −730 V at a pulse frequency of 20 kHz (50% duty cycle) were applied for plasma formation and ion beam acceleration, as previously reported.[27] First, an
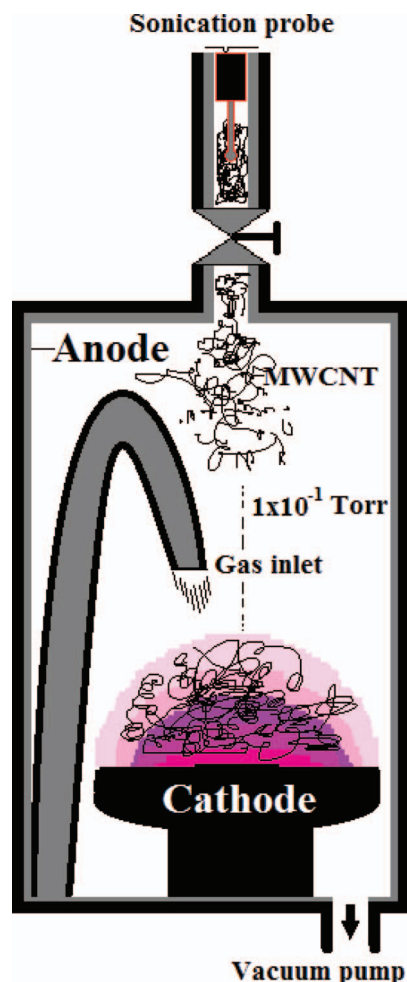
[z]E-mail: Hudson.Zanin@bristol.ac.uk

Figure 1. A schematic diagram showing the experimental setup.

argon plasma atmosphere at ∼13.3 Pa (Ar flow rate of 1 sccm) was produced and maintained for 1 h, as part of the substrate cleaning process. After that, a silane plasma (SiH$_4$ flow of 1 sccm) was maintained for a half-hour to form a conducting and well-adherent amorphous silicon interface. For DLC preparation, *n*-hexane acted as the source of carbon, and this was sprayed into the active plasma region via a nozzle which directed downwards onto the substrate surface for 1 hour, with Ar flowing during the whole process. For MWCNT incorporation, a suspension of 5 mg of MWCNT powder in 50 ml of *n*-hexane was made up. A special ultrasonic probe kept this MWCNT/hexane dispersion homogenized during the whole deposition process, and this suspension was sprayed into the chamber, as before.

The samples were characterized by high-resolution scanning electron microscopy (HR-SEM), Raman spectroscopy, spectral transmittance $T(\lambda)$, profilometry, scratching and electrochemical tests. HR-SEM was performed with a FEI Inspect F50 operated at 20–30 kV. Raman spectra were recorded at room temperature using a Renishaw microprobe, employing argon-ion laser excitation ($\lambda = 514.5$ nm) with a laser power of ∼6 mW and a spot size ∼5 μm. Curve fitting and data analysis Fityk software was used to assigned the peak locations and fit all spectra. A Hitachi U3501 spectrophotometer was employed to acquire transmittance spectra from 185 to 3200 nm. The film morphology and roughness values were characterized by a Wyko NT1100 optical profiler. In this study, a micro-scratch test was conducted on test samples using a 200 μm radius conical tip diamond stylus (Rockwell C 120°). The scratch test was carried out by drawing a diamond stylus tip three times across a sample at room temperature. The load was linearly increased within each pass until the coating was

stripped clean from the substrate. The load at which the coating was stripped from the substrate was termed the critical load. If the coating peeled off from the substrate surface while the stylus tip passed over it, the adherence was considered weak. Alternatively, if the coating only cracked in a roughly semicircular arc along the scratch without peeling off, the adherence was considered good. The test has already been used by a number of groups to study hard, thin, well-adhering coatings.[28–30]

A standard three-electrode cell was set up to evaluate the room temperature electrochemical performance of the DLC/MWCNT electrodes in a potentiostat (Autolab PGSTAT302N). The DLC/MWCNT electrode was characterized by cyclic voltammetry (CV) and electrochemical impedance spectroscopy (EIS). The electrical contact of the working electrodes was placed onto the stainless steel substrate using silver paint, with Teflon tape used to seal it. High-purity platinum wire and Ag/AgCl (3M KCl) were employed as counter electrodes and reference electrodes, respectively. All electrochemical experiments were carried out exposing a constant geometric area of 0.07 cm^2 (3 mm diameter) of the working electrode.

We evaluated different aspects of the electrochemical performance using 0.1 M potassium nitrate (KNO$_3$) as electrolyte and 0.5 mM ferrocene methanol (C$_{11}$H$_{12}$FeO) as a probe in aqueous solutions.[31] All chemicals were bought from Aldrich and used without further purification. The CV measurements were carried out from 0.01 to 1 V s^{-1} at potentials from 0 to 0.5 V. A pre-treatment was performed in which the system was held at 0 V for 1 min to polarize the electrodes; and then a first scan was obtained at 0 V in the positive direction. Subsequent CV scans were taken, as normal, over the full voltage range and analyzed and fitted using General Purpose Electrochemical Systems (GPES) data-processing software from Eco Chemie. Impedance spectroscopy measurements were carried out at 5 mV amplitude, 10 kHz to 0.1 Hz frequency range and at either open circuit potential (OCP) or formal potential. Prior to the measurement, the cells were kept at OCP for 20 min before measurement. At the end of each measurement, the Kramers-Kronig test[32] was applied to evaluate the consistency (causality, linearity, and stability) of the EIS data.

Results and Discussion

Figure 2 shows typical Raman spectra of the DLC film, MWCNT powder and the DLC/MWCNT film. The deconvolution of those spectra show peaks and bands centered at ∼1250 cm^{-1}, ∼1345 cm^{-1} (D-band), 1480 (nanophase), ∼1540–1585 cm^{-1} (G-band) and 1611–1620 cm^{-1} (D′-band). The band at 1250 cm^{-1} can be attributed to iTA, LA or LO modes of the CNTs very close to the K point, or a convolution of them.[33,34] The origin of the 1480 cm^{-1} band can be correlated to nanosized carbon formation or *trans*-polyacetylene.[35] The D and D′ bands are both sp^2 domains attributed to the disorder and imperfection of the carbon crystallites.[36] The G band is assigned to one of the two E$_{2g}$ modes corresponding to stretching vibrations in the basal plane (sp^2 domains) of single-crystal graphite or graphene.[37]

The integrated intensity ratio I_D/I_G in the Raman spectra has been used to correlate the structural purity of graphitic materials to the graphite crystal domain size,[35] and it is useful for estimation of the sp^2/sp^3 ratio in DLC films.[1,38] In Figure 2 the spectrum from DLC showed two broad Gaussian bands centered at 1345 cm^{-1} and 1541 cm^{-1}, in which the I_D/I_G ratio is 0.5, corresponding to ∼45−55% sp^3 content.[38,39] The main characteristics of this DLC produced by our pulsed PECVD process are similar to amorphous carbon hydrogenated (a-C:H).[26–28,31] The first-order MWCNT Raman spectrum was fitted using Lorentzian shapes for the D, G and G″ bands, and Gaussian shapes for bands around 1250, 1480 and 1611 cm^{-1} (D′ shoulder),[36] which the I_D/I_G ratio is ∼0.55.[34,38–40] As might be expected, the Raman spectra of DLC/MWCNT films have characteristics from both DLC and MWCNT Raman.[38,40] The I_D/I_G ratio increases to ∼0.62, indicating ∼35–45% of sp^3 content in DLC/MWCNT sample, which is lower than DLC without nanotubes.[34,38,40,41]

The optical band gaps were also calculated from an optical transmittance measurement through both DLC and DLC/MWCNT films,
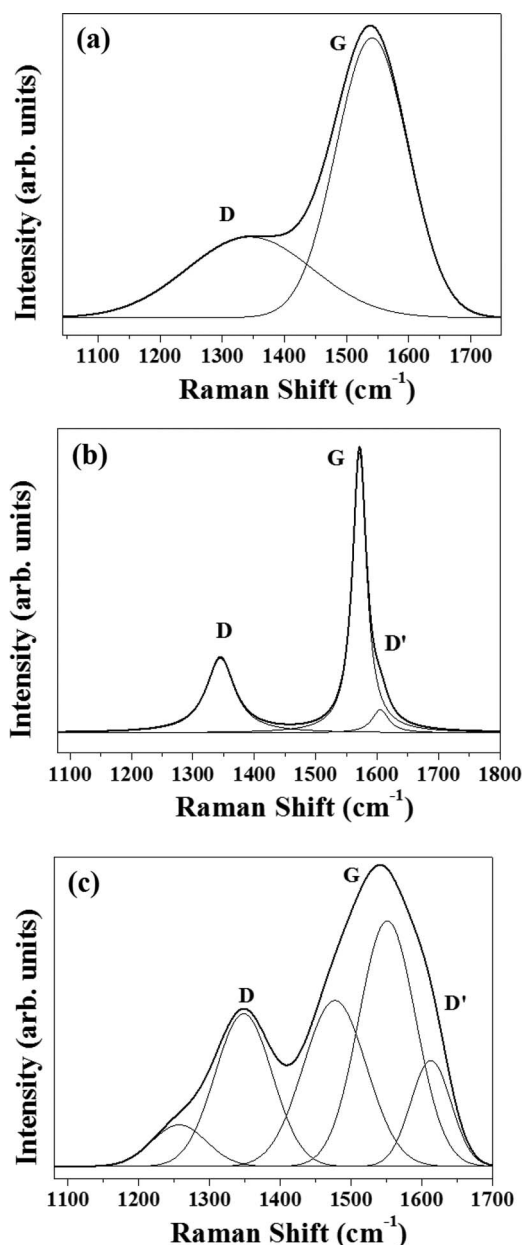
Figure 2. Raman spectra of the (a) DLC (b) MWCNT and DLC/MWCNT samples, showing the different peak contributions to the experimental spectra obtained from deconvolution by the fitting software.

which for these measurements were grown onto flat quartz substrates. The absorption constant was calculated from:

$$\alpha(E) = -(1/d)\ln(T(E)) \qquad [1]$$

where $\alpha(E)$ is the absorption constant, d is the thickness of the film (1 μm), T is the normalized optical transmittance and the wavelength, λ, is converted into photon energy E (eV) using the relation $E = (1240/\lambda)$. The band gaps were then obtained by a Tauc plot (Fig. 3) which involved plotting α^2 versus E, and extrapolating the linear part of the measurement to zero. We found that the incorporation of MWCNT into DLC films decreased the optical bandgap from $\sim$2.1 eV to $E \sim$1.9 eV, which is consistent with our previously work.[40]

Figures 4a & 4b show the typical morphology of DLC without nanotubes, revealing an amorphous film as smooth as the hand-polished stainless steel substrate surface. Figures 4c–4h show the effect of incorporation of MWCNT into DLC films. The surface is typically non-homogeneous (see Figure 5b), with nanotubes exposed
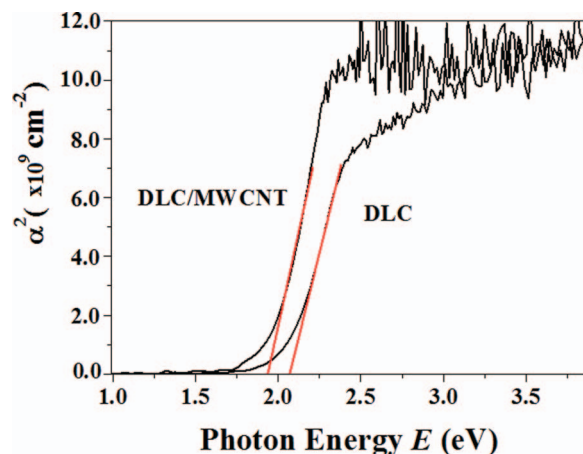

Figure 3. A Tauc plot for both DLC and DLC/MWCNT films grown onto quartz substrates. The dotted lines show the extrapolation to determine the bandgap.
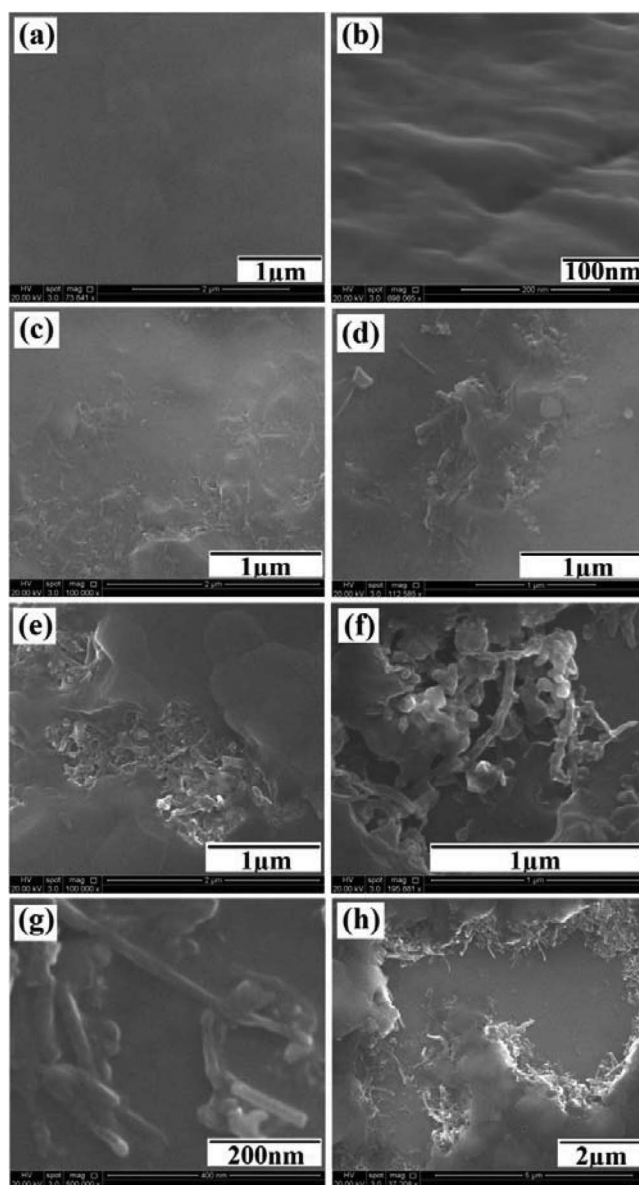

Figure 4. Scanning electron micrographs of the (a & b) DLC and (c to h) DLC/MWCNT films.
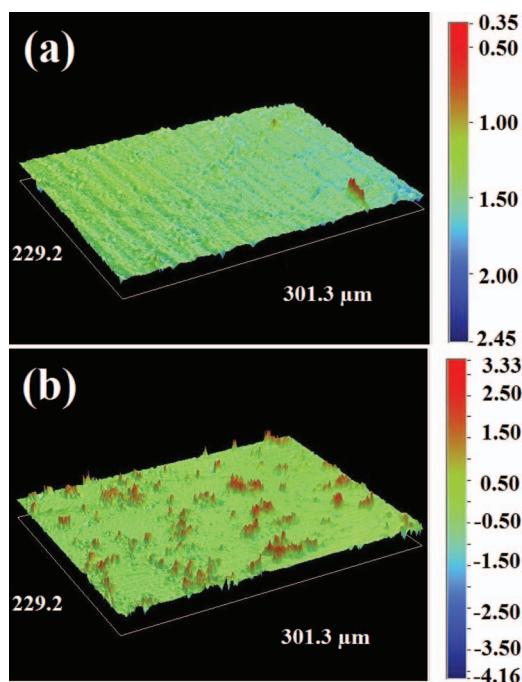
Figure 5. Profilometric images of (a) DLC and (b) DLC/MWCNT films. The height scale is color-coded in μm. The extra peaks in (b) are due to exposed CNTs which sometimes protrude through the DLC surface.

and protruding from the DLC film surface in many different regions. Figures 4d–4g present higher magnification details of the exposed nanotubes. Figure 4h shows a purpose-made defective region on that sample exposing the internal structure, and revealing that the MWC-NTs formed an interconnected web inside the DLC films. From those images, we estimated the CNT loading into the DLC of ∼25%.

Figure 5 shows the profilometric images of (a) DLC and (b) DLC/MWCNT film. The r.m.s. surface roughness of the DLC sample was 46 μm, which simply reflected the surface roughness of its respective substrate.[42] In contrast, the r.m.s. roughness of the DLC/MWCNT surface was higher (222 μm), consistent with the SEM images in Fig. 4.

Figure 6 presents results from the mechanical behavior of the DLC and DLC/MWCNT films following scratch testing. The graph shows the variation of the friction coefficient and acoustic emission with the force applied on the film. For this test a Rockwell tip was pressed against the surface of the film. The force applied was gradually increased with time throughout the test (up to 50 s). The film cracking is revealed by a significant sudden increase of both friction coefficient and acoustic emission. We confirmed the precise value for this by viewing video images of the sample during the test in real time. The force required to rupture the DLC film was ∼14 N, whereas for the DLC/MWCNT film this force value was ∼12 N. These results revealed the MWCNT incorporation decreases the film adherence by ∼15%. Nevertheless, the adherence remains high enough for the film to be viable for many applications. Figure 6 also shows that incorporation of MWCNTs significantly increased the DLC friction coefficient from 0.08 (DLC) to 0.2 (DLC/MWCNT), i.e. it made the films rougher; again consistent with the SEM images in Fig. 4 and profilometric images in Fig. 5.

Figure 7a & 7b shows the cyclic voltammograms from the DLC and DLC/MWCNT electrodes. In Fig. 7a we present voltammograms from both electrodes in 0.1 M KNO_3 and at 0.2 V s^{-1}. The voltammograms have a "quasi-rectangular" shape, which is typical of double layer formation.[36,43] The specific capacitance (SC) from DLC/MWCNT electrode is around 7 μF cm^{-2}, while SC from DLC we estimated to be a few nF cm^{-2}. Comparing those voltammograms, the DLC data produce a horizontal line, indicating lower capacitance due to the insulating behavior of DLC without nanotubes.

Fig. 7b shows voltammograms from a DLC/MWCNT electrode in ferrocene methanol solution performed at different scan rates from 0.2 to 1 V s^{-1}. The electrocatalytic activity has a significant low peak separation ($\Delta E \sim 62$ mV), indicating it exhibits fast electron transfer on its surface, as proposed for reversible process.[44] The ratio of anodic and cathodic peak currents is close to 1, the peak currents are inversely proportional to the square root of the scan rate and ΔE slightly increases as the scan rate increases. From these observations we conclude that the incorporation of the MWCNTs into DLC changes its insulating behavior and transforms it into a quasi-reversible electrode.

Electrochemical impedance analysis was performed on the DLC and DLC/MWCNT electrodes, and analyzed using Nyquist and Bode plots.[45,46] Figure 8 presents (a) the Nyquist plot of a DLC electrode in 0.1 M KNO_3 aqueous solution and (b) the Nyquist plot of DLC/MWCNT in 0.5 mM $C_{11}H_{12}FeO$ with 0.1 M KNO_3 aqueous
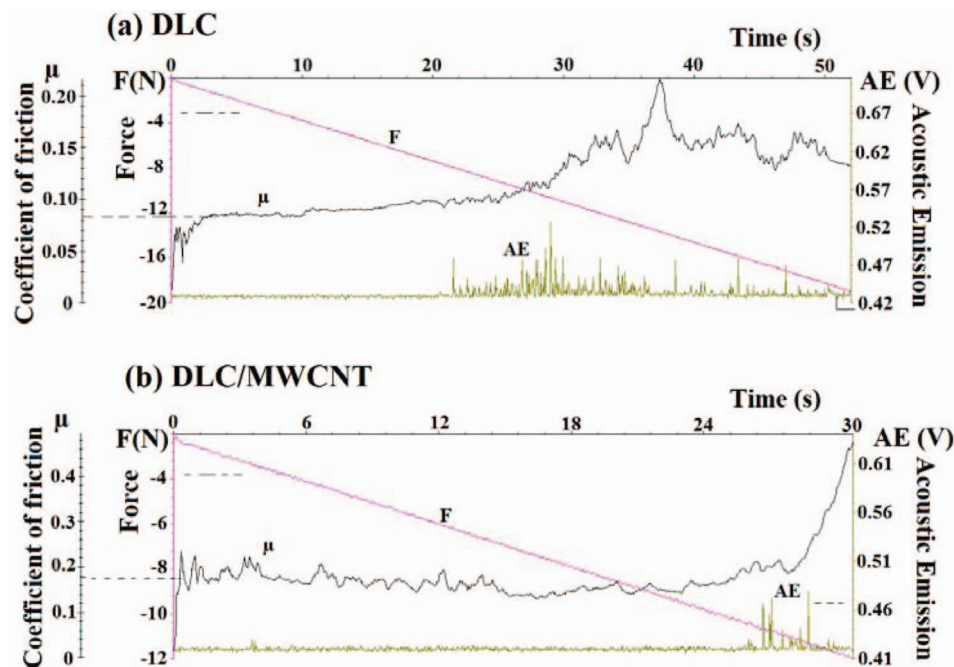

Figure 6. Scratch test results from (a) DLC and (b) DLC/MWCNT films, showing the applied force (F), the measured coefficient of friction (μ) and the acoustic emission (AE) against time.
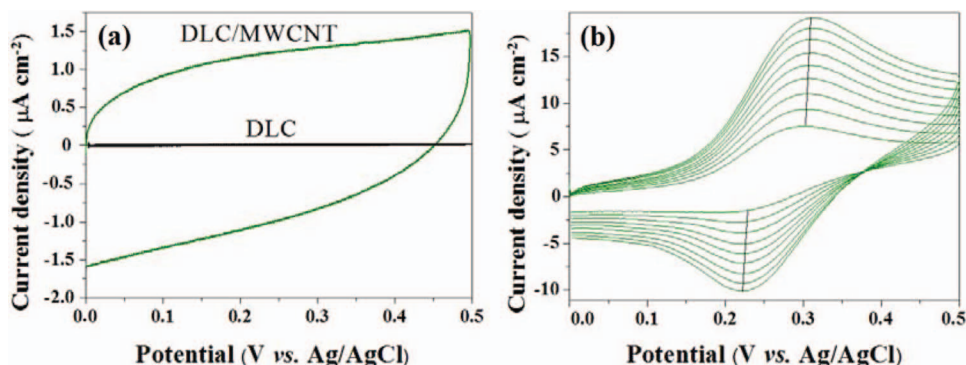
Figure 7. Cyclic voltammograms from (a) DLC and DLC/MWCNT electrodes at 0.1 M KNO$_3$ aqueous solution at 0.2 V s^{-1} and (b) DLC/MWCNT electrodes at 0.25 mM C$_{11}$H$_{12}$FeO and different scan rates from 0.2 to 1 V s^{-1}.

Table I. Electrochemical parameters extracted from DLC electrodes.

Sample	R_s (Ω)	C_{coat} (nF/cm^2)	R_{coat} (MΩ/cm^2)	C_{dl} (nF/cm^2)	R_p (GΩ/cm^2)	R_{ct} (kΩ/cm^2)
DLC	228 ± 7	5.8 ± 0.3	121 ± 7	9 ± 1	9.9 ± 0.5	–
DLC/MWCNT	232 ± 8			(7.2 ± 0.5) × 10^3	–	42 ± 3

solution; and (c) phase (d) amplitude plots from both measurements (a & b), with extracted data tabulated in Table I. From Fig. 8c & 8d, we can observe that the DLC is a capacitively insulating coating, which upon addition of CNTs becomes conductive and permits charge transfer on the surface. For the frequencies scanned, the modulus of the impedance of the DLC electrode ranges from 10^5 to 10^{10} Ω cm^{-2}, while that of the DLC/MWCNT electrode ranges from 10^3 to 10^5 Ω cm^{-2}. These electrochemical measurements indicate that the incorporation of the MWCNTs into DLC films considerably changes the conductivity behavior of DLC electrodes, improving conductivity and charge transfer.

To better interpret the Nyquist and Bode plots, they have been fitted using the equivalent electrical circuit (inset in Figs. 8a & 8b).[47,48] In these circuits, R_s is the internal resistance of the system, which consists of the ionic resistance of the electrolyte, the intrinsic resistance of the active material and the contact resistance at the electroactive material/current collector interface. Z_W represents the finite length Warburg impedance related to the diffusional (or mass transfer) impedance of electrochemical systems.[49] C_{dl} represents the non-faradaic charging of the electrical double layer using a constant phase element, CPE, given by CPE = $Q^{1/n}$, with Q being the charge and $n > 0.9$.[50] Thus, CPE is the effective capacitance of the double layer for nanostructured electrodes. R_{ct} represents the impedance for charge transfer and R_p the impedance for polarization.[31,48,51,52] The impedance data were fitted using the Zview software and the results are shown as the full lines in Figs. 8a–8c, while the extracted data are tabulated in Table I. From Table I we observe that the incorporation of nanotubes significantly increased the conductivity and the double layer formation of the DLC/MWCNT electrode.[53] In particular, the R_{ct} value is much lower than R_p and R_{coat}, which confirm that the incorporation of nanotubes allows fast charge transfer. In addition, nanotube incorporation increases the capacitance of DLC from nF cm^{-2} to μF cm^{-2}, because of the increase of both the electro-active area and the conductivity. Those values of capacitance extracted from CV are comparable to those from EIS.

Considering the CNT length is up to $\sim$40 μm and the thickness of the DLC film around 1 μm, we suggest the nanotubes create a dense interconnected network of CNTs within the DLC. This network creates conductive pathways which transport current rapidly to all parts of the film, including the surface regions where they can contribute to electrochemical redox reactions.

Conclusions

In this paper we present, for the first time, the incorporation of multi-walled carbon nanotubes into DLC films to improve their electrochemical characteristics, but without significant loss of mechanical properties or adherence. When used as an electrochemical electrode, this novel hybrid CNT/DLC material shows electro-catalytic activity for ferrocene methanol with fast charge transfer measured by CV and confirmed by EIS. Our electrochemistry results in potassium nitrate confirm the hypothesis that the incorporation of MWCNTs was largely responsible for the impedance reductions and the capacitance increases of the DLC films.

In these preliminaries experiments, it was not possible to control the amount of MWCNTs incorporated into the DLC film, and more studies are necessary to solve this issue. It is also necessary to improve the technique for producing more homogeneous samples. With this target in mind, we are improving our depositing system and we are
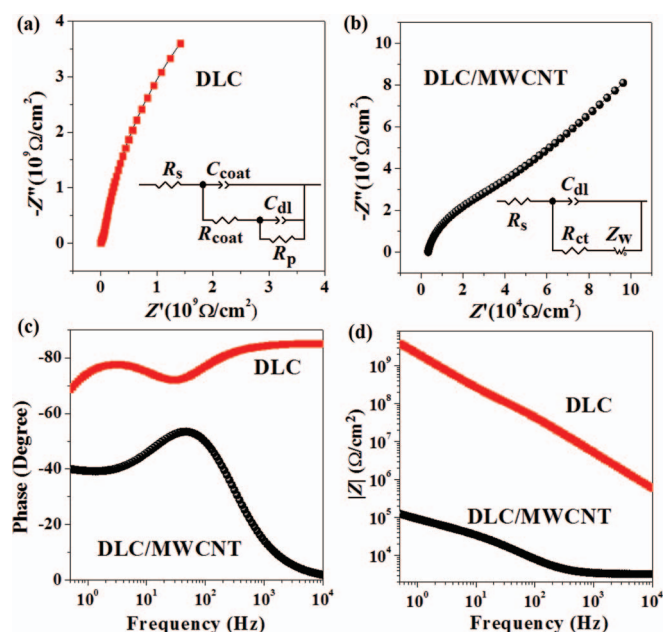

Figure 8. Nyquist plots taken over the frequency range of 10 kHz to 0.1 Hz from (a) a DLC electrode at OCP (0.082 V) and (b) a DLC/MWCNT electrode at its formal potential 0.259 V. (c) Bode plots from both (a) and (b).

studying new application for this new material such as the bioactivity, anti-bactericidal and the electrochemical sensitivity of this electrode for detection of chemicals in aqueous solutions.

References

1. J. Robertson, *Materials Science and Engineering R-Reports*, **37**, 129 (2002).
2. A. M. M. Omer, S. Adhikari, S. Adhikary, M. Rusop, H. Uchida, T. Soga, and M. Umeno, *Diamond and Related Materials*, **15**, 645 (2006).
3. S. Adhikary, X. M. Tian, S. Adhikari, A. M. M. Omer, H. Uchida, and M. Umeno, *Diamond and Related Materials*, **14**, 1832 (2005).
4. H. Dimigen, H. Hübsch, and R. Memming, *Applied Physics Letter*, **50**, 1056 (1987).
5. C. W. Chen and J. Robertson, *Carbon*, **37**, 839 (1999).
6. R. G. Compton, J. S. Foord, and F. Marken, *Electroanalysis*, **15**, 1349 (2003).
7. Y. Hayashi, S. Ishikawa, T. Soga, M. Umeno, and I. Jimbo, *Diamond and Related Materials*, **12**, 687 (2003).
8. M. Rusop, S. M. Mominuzzaman, T. Soga, T. Jimbo, and M. Umeno, *Japanese Journal of Applied Physics* Part 1-Regular Papers Short Notes & Review Papers, **42**, 2339 (2003).
9. V. S. Veerasamy, G. A. J. Amaratunga, C. A. Davis, A. E. Timbs, W. I. Milne, and D. R. McKenzie, *Journal of Physics-Condensed Matter*, **5**, L169 (1993).
10. A. Erdemir and C. Donnet, *Journal of Physics D-Applied Physics*, **39**, R311 (2006).
11. J. C. Sánchez-López, *A. Fernández Doping and Alloying Effects on DLC Coatings:Tribology of Diamond-Like Carbon Films*, Springer 2008, 311-338
12. M. AllonAlaluf and N. Croitoru, *Diamond and Related Materials*, **6**(5-7), 555 (1997).
13. Q. Wei, R. J. Narayan, J. Narayan, J. Sankar, and A. K. Sharma, *Materials Science and Engineering B-Solid State Materials for Advanced Technology*, **53**, 262 (1998).
14. Q. Wei, J. Sankar, A. K. Sharma, S. Oktyabrsky, J. Narayan, and R. J. Narayan, *Journal of Materials Research*, **15**, 633 (2000).
15. H. Hu, G. Chen, and J. Zha, *Surface and Coatings Technology*, **202**, 5943 (2008).
16. C. Wei, C.-I. Wang, F.-C. Tai, K. Ting, and R.-C. Chang, *Diamond and Related Materials*, **19**, 562 (2010).
17. H. Kinoshita, I. Ippei, H. Sakai, and N. Ohmae, *Diamond and Related Materials*, **16**, 1940 (2007).
18. C. Wei and J.-F. Yang, *Journal of Materials Research*, **27**, 330 (2012).
19. L. X. Liu and E. Liu, *Surface and Coatings Technology*, **198**, 189 (2005).
20. E. Liu and H. W. Kwek, *Thin Solid Films*, **516**, 5201 (2008).
21. R. Maalouf, H. Chebib, Y. Saikali, O. Vittori, M. Sigaud, F. Garrelie, C. Donnet, and N. Jaffirezic-Renault, *Talanta*, **72**, 310 (2007).
22. J.-I. Kim, A. Bordeanu, and J.-C. Pyun, *Biosensors and Bioelectronics*, **24**, 1394 (2009).
23. R. Schnupp, R. Kuhnhold, G. Temmel, E. Burte, and H. Ryssel, *Biosensors and Bioelectronics*, **13**, 889 (1998).
24. M. A. V. M. Grinet, H. Zanin, A. E. C. Granato, M. Porcionatto, F. R. Marciano, and A. O. Lobo, *Journal of Materials Chemistry B*, **2**, 1196 (2014).
25. A. O. Lobo, H. Zanin, I. A. W. B. Siqueira, N. C. S. Leite, F. R. Marciano, and E. J. Corat, *Materials science and engineering. C*, **7**, 4305 (2013).
26. R. P. C. C. Statuti, P. A. Radi, L. V. Santos, and V. J. Trava-Airoldi, *Wear*, **267**, 1208 (2009).
27. F. R. Marciano, L. F. Bonetti, D. A. Lima-Oliveira, C. B. Mello, M. Ueda, E. J. Corat, and V. J. Trava-Airoldi, *Diamond and Related Materials*, **19**, 1139 (2010).
28. L. V. Santos, V. J. Trava-Airoldi, E. J. Corat, J. Nogueira, and N. F. Leite, *Surface and Coatings Technology*, **200**, 2587 (2006).
29. D. Sheeja, B. K. Tay, S. P. Lau, and X. Shi, *Wear*, **249**, 433 (2001).
30. N. Dwivedi, S. Kumar, and H. K. Malik, *Journal of Applied Physics*, **111**(1), 014908 (2012).
31. H. G. Zanin, P. W. May, D. J. Fermin, D. Plana, S. M. C. Vieira, W. I. Milne, and E. J. Corat, *ACS applied materials and interfaces*, **6**(2), 990 (2014).
32. B. A. Boukamp, *Journal of the Electrochemical Society*, **142**, 1885 (1995).
33. R. Saito, A. Jorio, A. G. Souza, A. Grueneis, M. A. Pimenta, G. Dresselhaus, and M. S. Dresselhaus, *Physica B-Condensed Matter*, **323**, 100 (2002).
34. A. C. Ferrari and J. Robertson, *Philos. Trans. R. Soc. London, Ser. A*, **362**, 2477 (2004).
35. J. Tsukada, H. Zanin, L. C. A. Barbosa, G. A. da Silva, H. J. Ceragioli, A. C. Peterlevitz, R. F. Teofilo, and V. Baranauskas, *Journal of the Electrochemical Society*, **159**, D159 (2012).
36. E. F. Antunes, A. O. Lobo, E. J. Corat, V. J. Trava-Airoldi, A. A. Martin, and C. Verissimo, *Carbon*, **44**, 2202 (2006).
37. H. Zanin, E. Saito, H. J. Ceragioli, V. Baranauskas, and E. J. Corat, *Materials Research Bulletin*, **49**, 487 (2014).
38. A. A. Evtukh, H. Hartnagel, V. G. Litovchenko, M. Semenenko, and O. Yimazoglu, *Semiconductor Science and Technology*, **19**, 923 (2004).
39. M. A. Tamor and W. C. Vassell, *Journal of Applied Physics*, **76**, 3823 (1994).
40. H. Zanin, P. W. May, M. H. M. O. Hamanaka, and E. J. Corat, *ACS Appl. Mater. Interfaces*, **5**, 12238 (2013).
41. P. K. Chu and l. Li, *Mater. Chem. Phys.*, **96**, 253 (2006).
42. M. Zhong, C. Zhang, and J. Luo, *Applied Surface Science*, **254**, 6742 (2008).
43. L. Sun, C. Tian, M. Li, X. Meng, L. Wang, R. Wang, J. Yin, and H. Fu, *Journal of Materials Chemistry A*, **1**, 6462 (2013).
44. C. M. A. Brett and A. M. O. Brett, Electrochemistry: Principles, Methods, and Applications Oxford Science Publications, Oxford, 1993. - A. J. Bard and L. R. Faulkner, *Electrochemical Methods: Fundamentals and Applications*, John Wiley & Sons, Inc., New York, 2001.
45. W. Stephen Tait, *An Introduction to Electrochemical Corrosion Testing for Practicing Engineers and Scientists*; W. Stephen Tait, 1994; PairODocs Publications; 2048 St. Clair, Racine, WI 53402.
46. Y. F. Xing, S. J. O'Shea, and S. F. Y. Li, *Journal of Electroanalytical Chemistry*, **542**, 7 (2003).
47. J. E. B. Randles, Kinetics of rapid electrode reactions. *Discussions of the Faraday Society*, **1**, 11 (1947).
48. T. A. Silva, H. Zanin, E. Saito, R. A. Medeiros, F. C. Vicentini, E. J. Corat, and O. Fatibello-Filho, *Electrochimica Acta*, **119**, 114 (2014).
49. J. Hernando, S. Q. Lud, P. Bruno, D. M. Gruen, M. Stutzmann, and J. A. Garrido, *Electrochimica Acta*, **54**, 1909 (2009).
50. S. M. Park and J. S. Yoo, *Analytical Chemistry*, **75**, 455A (2003).
51. P. Papakonstantinou, J. F. Zhao, A. Richardot, E. T. McAdams, and J. A. McLaughlin, *Diamond and Related Materials*, **11**, 1124 (2002).
52. A. Zeng, E. Liu, I. F. Annergren, S. N. Tan, S. Zhang, R. Hing, and J. Gao, *Diamond and Related Materials*, **11**, 160 (2002).
53. H. E. Stanley, J. S. Andrade, S. Havlin, H. A. Makse, and B. Suki, *Physica A*, **266**, 5 (1999).